Available online at www.sciencedirect.com
SCIENCE DIRECT®
Applied Thermal Engineering 25 (2005) 31–44
APPLIED THERMAL ENGINEERING
www.elsevier.com/locate/apthermeng

A comparative study of five low Reynolds number k–ε models for impingement heat transfer

S.J. Wang *, A.S. Mujumdar

Department of Mechanical Engineering, National University of Singapore, 9 Engineering Drive 1, Singapore 119260, Singapore

Received 4 March 2004; accepted 1 June 2004
Available online 5 August 2004

Abstract

Five versions of low Reynolds number k–ε models for the prediction of the heat transfer under a two-dimensional turbulent slot jet were analyzed by comparison with the available experimental data. The Yap correction proposed for reducing the turbulence length scale in the near wall region was also tested with low Reynolds number k–ε models and found that for most of the models tested it is capable of improving the predicted local Nusselt number in good agreement with the experimental data in both stagnation and wall jet regions. Effects of the magnitudes of the turbulence model constants were also carried out for two low Reynolds number k–ε models and found that the set of model constants identical to those in the high Reynolds number k–ε model performs better than the original ones for jet impingement configurations. Finally, the effect of three jet inlet velocity profiles on the heat transfer rate was evaluated.

Keywords: Low Reynolds number k–ε model; Impinging jet; Turbulence modeling; Impingement heat transfer

1. Introduction

Single or multiple impinging jet (IJ) configuration provides high heat and mass transfer rates and hence various IJ geometric configurations have been widely used in a number of industrial areas ranging from thermal drying of continuous sheets (e.g. tissue paper, textiles, films, coated paper, veneer, lumber, etc.) and production of foodstuffs to electronic component cooling, annealing of metal sheets, tempering of glass, and cooling of turbine vanes. Over the past 30 years,

* Corresponding author.
E-mail address: g0202482@nus.edu.sg (S.J. Wang).

1359-4311/$ - see front matter
doi:10.1016/j.applthermaleng.2004.06.001

Nomenclature

C	turbulence length scale
C_μ, C_1, C_2	turbulence model constants
c_p	specific heat
f_μ, f_1, f_2	damping functions
H	nozzle-to-plate spacing
h	surface heat transfer coefficient
I	turbulence intensity
k	thermal conductivity
k	turbulent kinetic energy
l	turbulence length scale
l_e	near-wall equilibrium length scale
p	static pressure
T	temperature
u_i, u_j	velocity component in x and y directions
v_j	jet velocity component in y direction
U_i, U_j	time-averaged velocity component in x and y directions
W	slot width
x_i, x_j	coordinates
y^+	dimensionless distance $y^+ = u_\tau y\rho/\mu$

Greek symbols

μ, μ_t	laminar and eddy viscosities
v, v_t	laminar and eddy kinematic viscosities
ρ	density
ε	dissipation rate of turbulent kinetic energy
σ_k, σ_ε	turbulent Prandtl numbers

Dimensionless group

Re	jet Reynolds number based on jet inlet velocity and hydraulic diameter $Re = \rho v_j W/\mu$
Re_T, Re_y	turbulence Reynolds numbers
Nu	Nusselt number $N_u = hW/k$

Subscripts

$'$	fluctuation
avg	average
j	jet inlet
imp	impingement surface
ref	reference
yp	first grid near the wall

experimental and numerical investigations of flow and heat transfer characteristics under single or multiple impinging jets remain a very dynamic research area. The effects of nozzle geometry, jet-

to-surface separation, jet-to-jet separation, cross flow, operating conditions, etc. on flow and heat transfer have been experimentally studied [1–5]. Polat presented a detailed review of effects of the above important parameters on impingement transport phenomena [6].

Huang et al. [7] gave a comprehensive literature review on the subject of impingement heat transfer in both experimental and numerical aspects. They highlighted that the standard k–ε model with various wall functions fails to predict the stagnation heat transfer accurately and that the low Reynolds number k–ε models as well as advanced turbulent models are recommended to be tested for jet impingement flows characterized by strong streamline curvature, pressure gradients, and recirculation zones. Shi et al. [8] systematically studied the effects of turbulence models, near wall treatments, turbulent intensity, jet Reynolds number and boundary conditions on the heat transfer under a turbulent slot using the standard k–ε and RSM models. Their results indicate that both standard k–ε and RSM models predict the heat transfer rates inadequately, especially for low H/W aspect ratios. For wall-bounded flows, large gradients of velocity, temperature and turbulent scalar quantities exist in the near wall region and thus to incorporate the viscous effects it is necessary to integrate equations through the viscous sublayer using finer grids with the aid of turbulence models. Hossinalipour and Mujumdar [9] performed a comparative evaluation of different turbulent models for a confined impingement configuration with an aspect ratio of $H/W = 1.5$. They found the stagnation zone is difficult to predict accurately with any k–ε models, but the predicted local Nusselt numbers obtained using low Reynolds number k–ε models in stagnation zone are in good agreement with the experimental data. Thakre and Joshi [10] evaluated 12 versions of low Reynolds number k–ε models and two low Reynolds number RSM models for heat transfer in turbulent pipe flows. Their comparative analysis between the k–ε models and RSM models for the Nusselt number prediction is in favor of the applicability of the k–ε models even though the RSM model overcomes the assumption of isotropy and the constancy of turbulent Prandtl number.

Over the past few years, the low Reynolds number k–ε models have been widely used to predict wall-bounded flows due to its simplicity and to some extent capability of predicting the near wall flow and heat transfer characteristics by incorporating the damping functions. Since heat flux transport is more complicated than momentum transport, prediction of the heat transport still remains a challenging problem even under a single slot jet. The objective of this study is to investigate the relative performance of various versions of low Reynolds k–ε models in predicting the flow and heat transfer characteristics for impinging jet (IJ) configurations by comparison with available experimental data using CFD code FLUENT 6.1.18.

2. Mathematical model

In the present study, it is assumed that the fluid (air) is incompressible and Newtonian with temperature-dependent fluid properties. A numerical solution of the mean flow and thermal fields shown in Fig. 1 requires resolving the continuity equation (1), Reynolds averaged Navier–Stokes equation (2) and time-averaged energy equation (3):

$$\frac{\partial U_i}{\partial x_i} = 0 \tag{1}$$

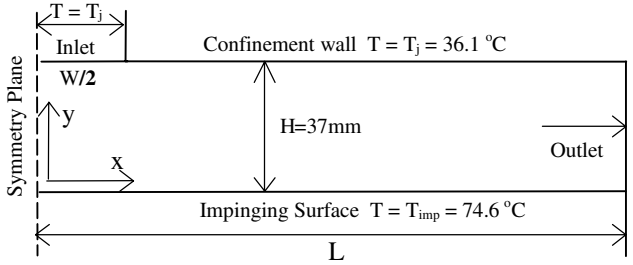

Fig. 1. Schematic configuration of the impinging jet configuration.

$$\rho U_i \frac{\partial U_j}{\partial x_i} = -\frac{\partial P}{\partial x_j} + \frac{\partial}{\partial x_i}\left[\mu\left(\frac{\partial U_i}{\partial x_j} + \frac{\partial U_j}{\partial x_i}\right) - \rho\overline{u_i' u_j'}\right] \tag{2}$$

$$\rho c_p U_i \frac{\partial T}{\partial x_i} = \frac{\partial}{\partial x_i}\left[k\frac{\partial T}{\partial x_i} - \rho\overline{u_i' T'}\right] \tag{3}$$

Based on the Boussinesq approximation, the Reynolds stress is related to the local velocity gradients by an eddy viscosity v_t. The turbulence scalar quantities (k and ε) used to calculate v_t are determined from the following modeled transport equations:

$$\rho U_i \frac{\partial k}{\partial x_i} = \frac{\partial}{\partial x_i}\left[\left(\mu + \frac{\mu_t}{\sigma_k}\right)\frac{\partial k}{\partial x_i}\right] + \mu_t\left(\frac{\partial U_i}{\partial x_j} + \frac{\partial U_j}{\partial x_i}\right)\frac{\partial U_i}{\partial x_j} - \rho\bar{\varepsilon} \tag{4}$$

$$\rho U_i \frac{\partial \varepsilon}{\partial x_i} = \frac{\partial}{\partial x_i}\left[\left(\mu + \frac{\mu_t}{\sigma_\varepsilon}\right)\frac{\partial \varepsilon}{\partial x_i}\right] + f_1 C_1 \mu_t \frac{\varepsilon}{k}\left(\frac{\partial U_i}{\partial x_j} + \frac{\partial U_j}{\partial x_i}\right)\frac{\partial U_i}{\partial x_j} - \rho f_2 C_2 \frac{\varepsilon^2}{k} + E \tag{5}$$

$$\mu_t = \rho f_\mu C_\mu \frac{k^2}{\varepsilon} \tag{6}$$

$$\bar{\varepsilon} = \varepsilon + D \tag{7}$$

$$Re_T = \frac{\rho k^2}{\mu\varepsilon}; \quad Re_y = \frac{\rho\sqrt{k}y}{\mu}; \quad Re_\varepsilon = \frac{\rho(\mu\varepsilon/\rho)^{1/4}y}{\mu} \tag{8}$$

where C_μ, C_1, C_2, σ_k and σ_ε are the same empirical turbulence model constants to those conventionally in the high Reynolds number k–ε model. The damping functions f_μ, f_1 and f_2, and in some modes the D and E terms are used to make the low Reynolds number models valid in the near wall region. The detailed physical meaning of these damping functions and the D and E terms as well as the criteria for examining the validity of these functions in the near wall region were given in Ref. [11]. Tables 1 and 2 summarize the five basic constants and the damping functions for the various low Reynolds number k–ε models.

Five low Reynolds k–ε models tested were those developed by Abid (thereafter referred to as AB) [12], Lam and Bremhorst (thereafter referred to as LB) [13], Launder and Sharma (thereafter referred to as LS) [14], Abe, Kondoh and Nagano (thereafter referred to as AKN) [15], and Change, Hsieh and Chen (thereafter referred to as CHC) [16,17], respectively.

Table 1
Summary of model constants and functions appearing in governing equations

Model	D	E	$\varepsilon_w - B.C.$	C_μ	C_1	C_2	σ_k	σ_ε
AB	0	0	$\varepsilon_w = \nu\left(\frac{\partial^2 k}{\partial y^2}\right)$	0.09	1.44	1.92	1.0	1.3
AB1				0.09	1.45	1.83	1.0	1.4
LB	0	0	$\left(\frac{\partial \varepsilon}{\partial y}\right)_w = 0$	0.09	1.44	1.92	1.0	1.3
LS	$2\nu\left(\frac{\partial \sqrt{k}}{\partial y}\right)^2$	$2\mu\nu_t\left(\frac{\partial^2 U}{\partial y^2}\right)^2$	0	0.09	1.44	1.92	1.0	1.3
AKN	0	0	$\varepsilon_w = \nu\left(\frac{\partial^2 k}{\partial y^2}\right)$	0.09	1.44	1.92	1.0	1.3
AKN1				0.09	1.5	1.9	1.4	1.4
CHC	0	0	$\varepsilon_w = \nu\left(\frac{\partial^2 k}{\partial y^2}\right)$	0.09	1.44	1.92	1.0	1.3

Table 2
Summary of damping functions appearing in the governing equations

Model	f_μ	f_1	f_2
AB	$f_\mu = \tanh(0.008 Re_y)\left(1 + 4 Re_T^{-3/4}\right)$	1.0	$[1 - 2/9\exp(-Re_T^2)/36]^2$ $[1 - (Re_y/12)]$
LB	$[1 - \exp(-0.0165 Re_T)]^2$ $[1 + (20.5/Re_y)]$	$1 + (0.005/f_\mu)^3$	$1 - \exp(-Re_T^2)$
LS	$\exp[-3.4/(1 + Re_T/50)^2]$	1.0	$1 - 0.3\exp(-Re_T^2)$
AKN	$\{1 + 5.0/Re_T^{3/4}\exp[-(Re_T/200)^2]\}$ $[1 - \exp(-Re_\varepsilon/14)]^2$	1.0	$\{1 - 0.3\exp[-(Re_T/6.5)^2]\}$ $[1 - (Re_\varepsilon/3.1)]^2$
CHC	$[1 - \exp(-0.0215 Re_y)]^2\left(1 + 31.66/Re_T^{5/4}\right)$	1.0	$[1 - 0.01\exp(-Re_T^2)]$ $[1 - \exp(-0.0631 Re_y)]$

3. Problem description

A schematic representation of the slot jet impinging configuration is shown in Fig. 1. Due to geometric and physical symmetry, only the flow field within the half domain shown in Fig. 1 was solved numerically. The following boundary conditions were used: the impinging surface was specified as an isothermal wall; constant temperature equal to that of the jet was set to the top confinement wall; the uniform velocity, temperature, turbulent kinetic energy and energy dissipation rate profiles were assumed at the nozzle exit; symmetry and outflow boundary conditions were assumed at symmetry and outlet planes; the no-slip condition were specified on the confinement walls. Without special statement, turbulence intensity and length scale at the nozzle exit were set to be 2% and 0.07 W [18], respectively.

In the interest of accuracy, the governing equations were discretized using a second order upwind interpolation scheme in FLUENT [18]. The convergence criteria were specified as follows: the normalized residuals of all dependent variables must be less than 10^{-7}. To resolve the near wall region with large gradients satisfactorily, finer computational grids were set near the wall and y_{fp}^+ was kept less than unity for all cases. To ensure the attainment of grid-independent results, the sensitivities of both grid numbers and grid distributions were tested for each case. Fig. 2 shows

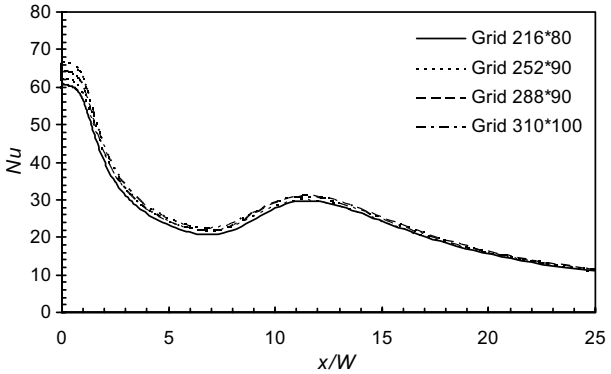

Fig. 2. Effect of grid size on the predicted Nusselt number, $Re = 10{,}400$, $H/W = 2.6$.

one of the results of effect of grid size on the predicted Nusselt number distribution. Typically, a grid density of 216*80 provides satisfactory solution for the example shown.

4. Results and discussion

Based on how detailed the authors described the experimental setup and procedures as well as the boundary conditions required for simulations, two sets of experimental data of the jet impingement flows were selected from the available literature as test cases. One was a case with low H/W ($=2.6$), the other was a case with high H/W ($=6.0$) [2].

4.1. Performance of various low Reynolds k–ε models

Fig. 3 shows a comparison of the streamwise local Nusselt number distribution predicted by five low Reynolds k–ε models with experimental data [2] at $Re = 10{,}400$ for $H/W = 2.6$. The local

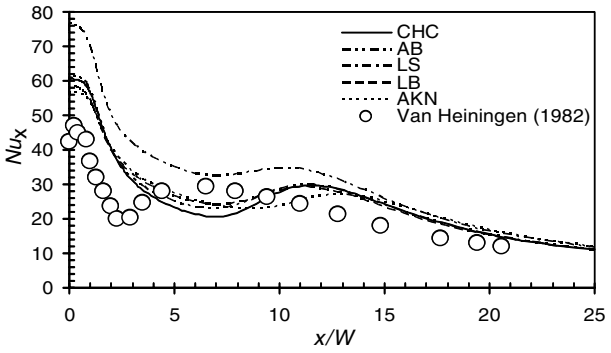

Fig. 3. Comparison of the predicted Nusselt number with experimental data, $Re = 10{,}400$, $H/W = 2.6$.

Nusselt number was defined as $Nu_x = h_x W/k$, where $h_x = q/(T_{imp} - T_{ref})$ and T_{imp} and T_{ref} are the impinging surface and jet inlet temperatures.

It is seen from Fig. 3 that all low Reynolds k–ε models tested capture the shape of the Nu_x profile quite well, but overestimate the magnitudes of Nu_x at both stagnation point and downstream points. The LS model performs worse than the other models in the range of $0 < x/W < 15$. All the models tested predict the position of the secondary Nu_x maximum inadequately. In the near wall region, the heat transfer rates are conduction-dominated where most of the temperature and velocity changes occurs, therefore the overestimation of Nu_x, especially in stagnation region, may be because the thickness of the conduction-dominated layer is reduced by the very large turbulence length scales used in the turbulence models. As consequence it reduces the overall thermal resistance across the flow and thus high heat transfer rates. Note that except for the special statement for the use of turbulence model constants in the AB and AKN models the coefficients of C_μ, C_1, C_2, σ_k and σ_ε used in the AKN and AB models were set the same to those in the standard high Reynolds number k–ε model (viz. 0.09, 1.44, 1.92, 1.0, 1.3). The reason for this change is that the validation of this conventional set of turbulence model constants has been widely tested and confirmed in the turbulent core region.

Except the AKN model, the other models predict similar dimensionless position of the secondary Nu_x maximum. When confined to the viscosity-affected region of the flow, it seems that the near-wall model greatly influences the wall heat transfer rates, but not much the position of the secondary Nu_x maximum.

Fig. 4 shows a comparison of the streamwise local Nusselt number distribution predicted by five low Reynolds k–ε models with experimental data [2] at $Re = 5200$ for $H/W = 6$. Again, it is seen that all the models are able to capture the shape of the Nu_x profile with a weak secondary Nu_x maximum reasonably well. The Nu_x predicted by the CHC, AB, LB and AKN models in the range of $0 < x/W < 10$ is in close accordance with experimental data, but is overestimated further downstream. Again, the LS model overestimates the Nu_x in the impinging and downstream regions. It may result from the fact that the damping function f_2 should reach its asymptotic value of unity at Reynolds number Re_T smaller than 15 and thus its effect is limited to the viscous sublayer [11]. However the damping function f_2 used in LS model does not display this near wall limiting behavior properly and has a slower decay than those in other models, hence the LS model

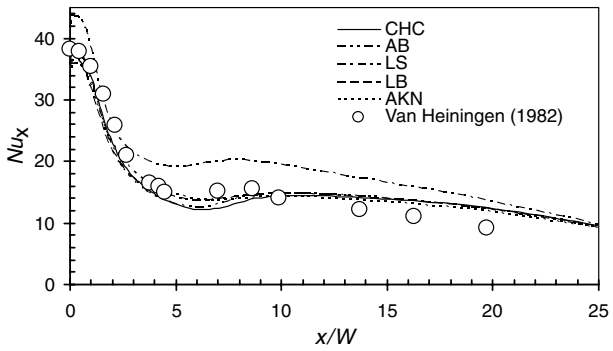

Fig. 4. Comparison of the predicted Nusselt number with experimental data, $Re = 5200$, $H/W = 6$.

tends to predict small energy dissipation rate near the wall and as consequence overestimates the Nusselt number more greatly when compared with other low Reynolds number models.

4.2. Performance of various low Reynolds k–ε models including Yap correction

Launder [19] noted that there exists a secondary source/sink term S_ε in the ε equation that is taken as zero in most studies. Yap [20] proposed the following source term that functions as the ratio of a computational length scale to the local equilibrium length scale:

$$S_\varepsilon = \max\left[0.83\left(\frac{l}{l_e}-1\right)\left(\frac{l}{l_e}\right)^2\frac{\varepsilon^2}{k},0\right]$$

where $l_e = Cy$ denotes the near-wall equilibrium length scale taken as 2.5 times the distance from the wall, here turbulence scale constant C is equal to $\kappa/C_\mu^{0.75} = 2.495$ and κ is the von Karman constant, while l introduces a turbulence length scale defined as $l = k^{3/2}/\varepsilon$. This source term vanishes in local-equilibrium wall turbulence due to $l = l_e$ and at large distance from the wall due to $l \ll l_e$. When $l > l_e$, the source term is positive and $(l/l_e)^2$ allows the required increases of values of ε and thus decreasing values of turbulence length scale l. Hosseinalipour and Mujumdar [9] first investigated in depth the effect of incorporating Yap correction in the ε equation of various low Reynolds k–ε models for $H/W = 1.5$ and $Re = 8000$. They found that the Yap correction improves the Nu_x prediction downstream to some extent for some of the tested models, but no improvement in the impinging region. In this study, the performance of Yap correction was tested for five low Reynolds number k–ε models with the aid of a user-defined function written in C programming language and macros supplied by FLUENT.

Fig. 5 shows a comparison of the predicted Nu_x using five low Reynolds number models with Yap correction (thereafter referred to as CHCY, ABY, LSY, LBY and AKNY, respectively) with experimental data [2] for $H/W = 2.6$ and $Re = 10{,}400$. Compared Fig. 5 with Fig. 3, it is seen that for all the models tested the Yap correction improves the prediction of Nu_x significantly. Except the LSY model, the predicted Nusselt numbers by the other four models with Yap correction are in good agreement with experimental data in both the impinging region and the downstream region ($x/W > 10$), but still predict Nu_x inadequately in the ranges of $2 < x/W < 10$. The LSY

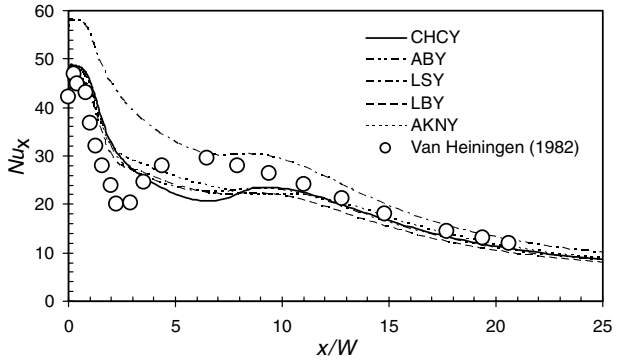

Fig. 5. Effect of Yap correction on the Nusselt number, $Re = 10{,}400$, $H/W = 2.6$.

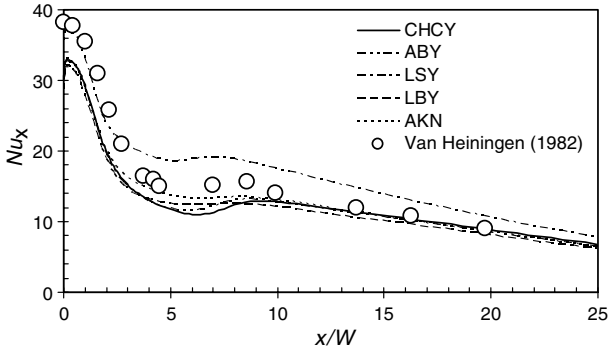

Fig. 6. Effect of Yap correction on the Nusselt number, $Re = 5200$, $H/W = 6$.

model still overestimates the Nu_x in the impinging region although the values of the predicted Nu_x in the impinging region are reduced greatly, but in good accordance with experimental data downstream. Except the CHCY model, the other four models fail to capture the secondary Nu_x maximum. The inadequacy of predicting Nu_x in the range of $2 < x/W < 10$ may be attributable to the transition of flow from laminar to turbulent. This may be the reason for the increase of the local Nusselt number to a secondary maximum [21].

Fig. 6 shows a comparison of the predicted Nu_x using five low Reynolds number models with Yap correction with experimental data for $H/W = 6$ and $Re = 5200$. Compared Fig. 6 with Fig. 4, it is seen that except the LSY model the other four models with Yap correction improve the downstream Nu_x in close agreement with the experimental data in the range of $x/W > 10$, but underestimate the Nu_x in the range of $0 < x/W < 10$. The LSY model predicts the Nu_x quite well in the range of $0 < x/W < 3$, but overestimates the Nu_x downstream.

4.3. Effect of turbulence intensity at the nozzle exit

Since higher level of turbulence intensity is generally associated with high heat transfer rate, the turbulence intensity characterizing the strength of turbulence at the nozzle exit should exert the effect on the heat transfer rate. In this study, the effect of increasing turbulence intensity from 1% to 6% on the heat transfer rate was studied using the CHC model with Yap correction for $H/W = 2.6$ and $H/W = 6$, respectively. Here, the turbulence intensity, I, is defined as the ratio of the root-mean-square of the velocity fluctuations, u', to the mean flow velocity, u_{avg}. Figs. 7 and 8 show that as the turbulent intensity increases from 1% to 6% the local Nusselt number increases appreciably in the impinging region and further downstream region, but decreases in the range of $x/W < 9$. For example, the maximum increase of Nusselt number in the stagnation point is 6.7% when turbulent intensity increases from 1% to 6%. However, Shi and Mujumdar [8] and Morris et al. [22] found that the turbulence intensity has no influence on the heat transfer and flow field predictions except near the stagnation region using the standard k–ε model. It may result mainly from the fact that in the standard k–ε model the wall function is used to bridge the effects of low Reynolds number and molecular viscosity in the near wall region as well as that the isotropy of Reynolds stress is assumed in the near wall region. In the work of Shi and Mujumdar [8], the effect

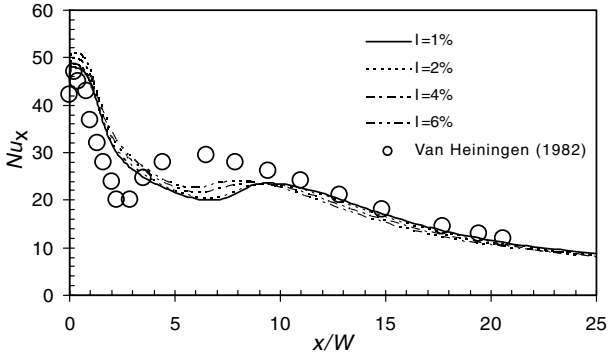

Fig. 7. Effect of turbulent intensity on the predicted Nusselt number against experimental data, $Re = 10{,}400$, $H/W = 2.6$.

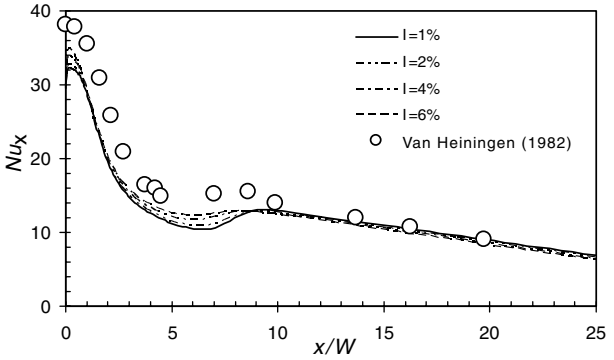

Fig. 8. Effect of turbulent intensity on the predicted Nusselt number against experimental data, $Re = 5200$, $H/W = 6$.

of the turbulence intensity shows appreciable effect on the heat transfer and flow field in both impinging region and downstream region using the standard RSM model. Similar effect of turbulent intensity on the heat transfer (not shown) is also found using other low Reynolds models.

4.4. Effect of turbulence model constants

Fig. 9 shows a comparison of the predicted local Nusselt number using two sets of turbulent model constants for the AB and AKN models. A set of turbulence model constants identical to that used in the standard k–ε model was used in the AB model, but the set of turbulence model constants in [12] was used in the AB1 model, and so did the AKN and AKN1 models. It is seen from Fig. 9 that the local Nu_x predicted by the models of AB1 and AKN1 are much away from the experimental data than those predicted by the AB and AKN models in both magnitudes of Nu_x and the position of the secondary Nu_x maximum. It may be because in the turbulent core region the molecular viscous effect becomes negligible and thus the set of turbulent model constants should be identical to that used in the standard k–ε model whose validity in the turbulent core

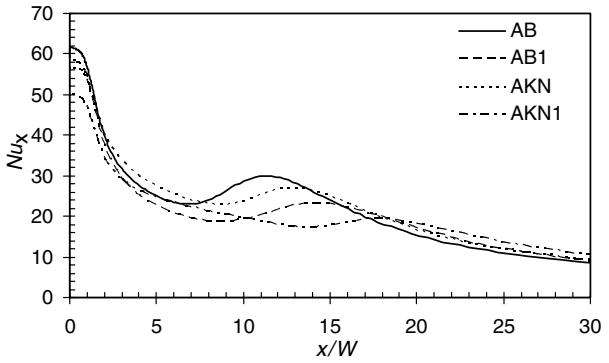

Fig. 9. Effect of turbulent model constants on the Nusselt number, $Re = 10{,}400$, $H/W = 2.6$.

region has been widely proven. Therefore use of the AB and AKN models is case-dependent due to the use of different turbulence model constants from those used in the standard k–ε model. However, in this work, the AB and AKN models with the use of turbulence model constants identical to those in the standard k–ε model predict the Nu_x comparable to those predicted by the CHC and LB models. The Nusselt number distributions obtained by two sets of turbulence model constants indicate that the turbulence model constants affect not only the heat transfer rates but the position of the secondary Nu_x maximum greatly.

4.5. Effect of inlet velocity profile

Simulations were carried out for three jet inlet velocity profiles using the CHC and the CHCY models. The detailed velocity profile expressions are shown in Table 3 and for a given operating condition and geometry the total mass flow rate for three velocity profiles were kept identically.

Figs. 10 and 11 show the effect of velocity profile on the local Nusselt number distributions for $H/W = 2.6$ at $Re = 10{,}400$ and $H/W = 6$ at $\mathrm{Re} = 5200$, respectively. In the interest of brevity, FlatV and FlatVY in Figs. 9 and 10 thereafter refer to the use of flat velocity profile without and with incorporating Yap correction into the CHC model and so do the other two velocity profiles. It is seen that the predicted Nu_x is much higher for the PV profile than for the FV and PLV profiles in and near the impinging regions. It is ascribed to the slower jet spreading rate for the PV profile at the inlet since the jet momentum is concentrated on the axis and thus having the strongest jet penetration capacity among the there velocity profiles tested. This results in high heat transfer rate in and near the impinging regions. This trend is reversed once a critical value of x/W is reached. It occurs because the air temperature increase due to the heat transfer in and near the impinging regions is higher for the PV profile than for the FV and PLV profiles and therefore

Table 3
Inlet velocity profile expressions

	Flat velocity (FV)	Power law velocity (PLV)	Parabolic velocity (PV)
v component	$v = v_{\mathrm{j}}$	$v = v_{\mathrm{j,max}}(W/2 - x)^{1/7}$	$v = v_{\mathrm{j,max}}[1 - (x/W/2)^2]$

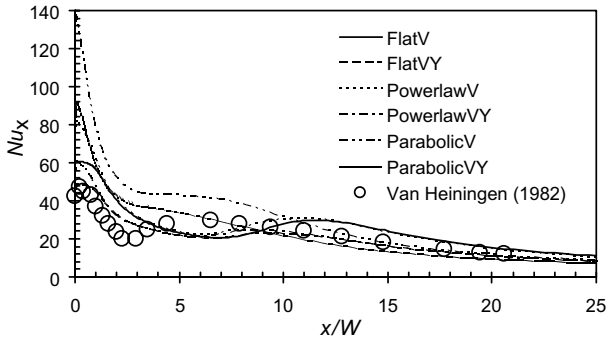

Fig. 10. Effect of inlet velocity profile on the Nusselt number, $Re = 10{,}400$, $H/W = 2.6$.

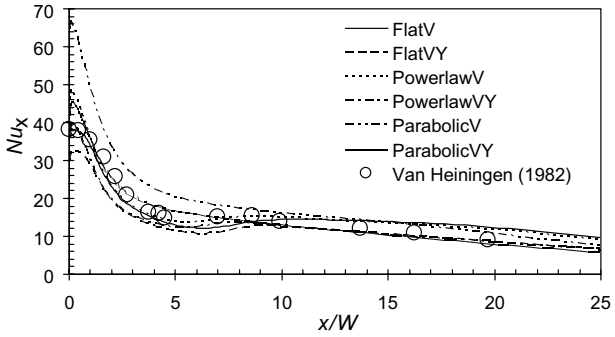

Fig. 11. Effect of inlet velocity profile on the Nusselt number, $Re = 5200$, $H/W = 6$.

decreasing the heat transfer rate after a critical value of x/W. Except the impinging region, the heat transfer rate difference is minor between the FV and PLV profiles since the power law turbulent velocity profile provides slightly slower jet spreading rate than the flat velocity profile. For all the cases here, the Yap correction can appreciably decreases the heat transfer rate, especially in and near the impinging regions.

5. Concluding remarks

A comparative study of the heat transfer under a turbulent slot jet was carried out using five low Reynolds number k–ε models. The predicted local Nusselt number distributions were compared with the available experimental data [2]. Some of the specific conclusions are summarized as follows:

- None of the low Reynolds number k–ε models tested are capable of predicting the local Nusselt number in good agreement with experimental results over the whole domain; all the models performs better for high H/W than low H/W;

- For AB, LB, AKN and CHC models, the Yap correction which decreases the turbulence length scale in the near wall region improves the predicted local Nusselt number in good agreement with the experimental data in both stagnation and further downstream regions, especially for low H/W, but still predicts the local Nusselt number in the ranges of $2 < x/W < 10$ inadequately;
- AKN and AB models with the set of turbulence model constants identical to those used in the standard k–ε model predict the local Nusselt number distributions with accuracy comparable to that obtained by LB and CHC models. Care should be exercised on use of these two models for different kinds of wall-bounded flows;
- Increasing the turbulence intensity from 1% to 6% at the nozzle exit shows only a slight effect on heat transfer over the whole domain;
- Regarding the relative performance of various low Reynolds number models tested for the jet impingement heat transfer, the CHC model capable of correctly yielding the near wall limiting flow behavior is believed to be more appropriate for wall bounded flows with strong streamline curvature and separated regions;
- The jet inlet velocity profile that provides slow jet spreading rate increases the heat transfer in and near impinging regions until a critical value of x/W is reached. For flat and power velocity profiles, the difference of heat transfer rate is minor except in the impinging region.

References

[1] N.R. Saad, Flow and heat transfer for multiple turbulent impinging slot jets, Ph.D. Thesis, Department of Chemical Engineering, McGill University, Montreal, Quebec, Canada, 1981.
[2] A.R.P. Van Heiningen, Heat transfer under an impinging slot jet, Ph.D. Thesis, Department of Chemical Engineering, McGill University, Montreal, Quebec, Canada, 1982.
[3] N.R. Saad, S. Polat, W.J.M. Douglas, Confined multiple impinging slot jets without crossflow effects, International Journal of Heat and Fluid Flow 13 (1) (1992) 2–14.
[4] G.K. Morris, S.V. Garimella, Orifice and impingement flow fields in confined jet impingement, Journal of Electric Packaging 120 (1998) 68–72.
[5] V. Narayanan, J.S. Yagoobi, R.H. Page, An experimental study of fluid mechanics and heat transfer in an impinging slot jet flow, International Journal of Heat and Mass Transfer 47 (2004) 1827–1845.
[6] S. Polat, Heat and mass transfer in impingement drying, Drying Technology 11 (6) (1993) 1147–1176.
[7] S. Plat, B. Huang, A.S. Mujumdar, W.J. Douglas, Numerical flow and heat transfer under impinging jets, Annual Review of Numerical Fluid Mechanics and Heat Transfer 2 (1989) 157–197.
[8] Y.L. Shi, M.B. Ray, A.S. Mujumdar, Computational study of impingement heat transfer under a turbulent slot jet, Industrial & Engineering Chemistry Research 41 (18) (2002) 4643–4651.
[9] S.M. Hosseinalipour, A.S. Mujumdar, Comparative evaluation of different turbulence models for confined impinging and opposing jet flows, Numerical Heat Transfer, Part A 28 (1995) 647–666.
[10] S.S. Thakre, J.B. Joshi, CFD modeling of heat transfer in turbulent pipe flow, The American Institute of Chemical Engineers 46 (9) (2000) 1798–1812.
[11] V.C. Patel, W. Rodi, G. Scheuerer, Turbulence models for near-wall and low Reynolds number flows: a review, The American Institute of Aeronautics and Astronautics 23 (9) (1985) 1308–1319.
[12] R. Abid, Evaluation of two-equation turbulence models for predicting transitional flows, International Journal of Engineering Science 31 (6) (1993) 831–840.
[13] C.K.G. Lam, K. Bremhost, A modified form of the k–ε model for prediction wall turbulence, Transactions of the ASME, Journal of Fluids Engineering 103 (1981) 456–460.

[14] B.E. Launder, B.I. Sharma, Application of the energy-dissipation model of turbulence to the calculation of flow near a spinning disc, Letters in Heat and Mass Transfer 1 (1974) 131–138.
[15] K. Abe, T. Kondoh, Y. Nagano, A new turbulence model for predicting fluid flow and heat transfer in separating and reattaching flows I: Flow field calculations, International Journal of Heat and Mass Transfer 37 (1) (1994) 139–151.
[16] K.C. Chang, W.D. Hsieh, C.S. Chen, A modified low-Reynolds-number turbulence model applicable to recirculating flow in pipe expansion, Transactions of the ASME, Journal of Fluids Engineering 117 (1995) 417–423.
[17] W.D. Hsieh, K.C. Chang, Calculation of wall heat transfer in pipe-expansion turbulence flows, International Journal of Heat and Mass Transfer 39 (18) (1996) 3813–3822.
[18] Fluent 6.1.18 User's Guide, Volumes 1–5, Fluent Inc., 2002.
[19] B.E. Launder, Current capabilities for modeling turbulence in industrial flows, Applied Scientific Research 48 (1991) 247–269.
[20] C.R. Yap, Turbulent heat and momentum transfer in recirculating and impinging flows, Ph.D. Thesis, Faculty of Technology, University of Manchester, 1987.
[21] S. Polat, Transport phenomena under jets impinging on a moving surface with through flow, Ph.D. Thesis, Department of Chemical Engineering, McGill University, Montreal, Quebec, Canada, 1988.
[22] G.K. Morris, S.V. Garimella, R.S. Amano, Prediction of jet impingement heat transfer using a hybrid wall treatment with different turbulent Prandtl number functions, Transactions of the ASME, Journal of Heat Transfer 118 (1996) 562–569.